Current Applied Science and Technology Vol. 22 No. 5 (September-October 2022)

Research article

The Effects of CsBr Concentration on the Inorganic Cesium Lead Bromide Perovskite Film Properties and the Performances of Carbon-Based HTM-Free Perovskite Solar Cells

Vallop Homrahad[1,2], Madsakorn Towannang[1,3,4], Pantiwa Kumlangwan[1,3,4], Wirat Jarernboon[1,3,4]*, Samuk Pimanpang[4,5] and Vittaya Amornkitbambung[1,3,4]

[1]Department of Physics, Faculty of Science, Khon Kaen University, Khon Kaen, Thailand
[2]Department of Physics, Faculty of Science, Buriram Rajabhat University, Buriram, Thailand
[3]Institute of Nanomaterials Research and Innovation for Energy (IN-RIE), Research Network of NANOTEC-KKU (RNN), Khon Kaen University, Khon Kaen, Thailand
[4]Thailand Center of Excellence in Physics (ThEP), PO Box 70 Chiang Mai University, Chiang Mai, Thailand
[5]Department of Physics, Faculty of Science, Srinakharinwirot University, Bangkok, Thailand

Received: 17 August 2021, Revised: 8 November 2021, Accepted: 20 December 2021

DOI: 10.55003/cast.2022.05.22.003

Abstract

Keywords

CsBr;

inorganic cesium lead bromide perovskite;

solar cells;

hole transport material free

Inorganic cesium lead bromide (ICLB) perovskite films were prepared onto an FTO conductive substrate by a two-step spin-dipping method. $PbBr_2$ films were first coated onto the FTO substrate, and then they were immersed into CsBr solutions at various concentrations: 0.04, 0.06, 0.08, 0.10, and 0.12 M, forming the ICLB perovskite films. The surface morphology of the perovskite films prepared from the CsBr concentrations under 0.08 M had a uniform crystalline surface, but the CsBr concentrations above 0.08 M gave the film a non-uniform structure. XRD spectra of all ICLB films compose of mixed phases of monoclinic-$CsPbBr_3$ and tetragonal-$CsPb_2Br_5$. The direct optical bandgap of 2.3 eV corresponded to the $CsPbBr_3$ phase, and the indirect optical bandgap of 2.87-3.10 eV corresponded to the $CsPb_2Br_5$ phase. Carbon-based hole-transport-material (HTM) free $CsPb_2Br_5$ - $CsPbBr_3$ perovskite solar cells were assembled, and the $CsPb_2Br_5$ - $CsPbBr_3$ perovskite solar cells prepared from 0.08 M CsBr concentration delivered the highest efficiency of 2.6%. This was because the 0.08 M-perovskite film had good uniformity, low pinhole defect, and low $PbBr_2$ impurities. Good cell stability, with an efficiency reduction of 10.0% of the initial value after 816 h under ambient environment, was achieved from the 0.08 M CsBr concentration cells.

*Corresponding author: Tel.: (+66) 866408352 Fax: (+66) 043202374
E-mail: wiratja@kku.ac.th

1. Introduction

Perovskite solar cell (PSCs) were first prepared from methylammonium lead triiodide ($CH_3NH_3PbI_3$) with a power-conversion efficiency (PCE) of 3.8% in 2009 [1-8]. Currently, the $CH_3NH_3PbI_3$ perovskite based solar cells have PCE of over 25.2% [9]. Although the $CH_3NH_3PbI_3$ perovskite based solar cells deliver outstanding performance, they are unstable in the open-air conditions. Niu *et al*. [10] reported that moisture degrades $MAPbI_3$ perovskites by decomposing them back to the methylammonium iodide salt (MAI) and metal halides. They proposed that $MAPbI_3$ perovskite is deprotonated by water, forming methylamine, hydrated HI, and PbI_2 byproducts. To solve the degradation problem, inorganic cesium lead bromide (ICLB) perovskite has received strong attention because it has good stability under moisture, oxygen and heat in the ambient air conditions [11-13]. ICLB-based perovskite films have been fabricated by various techniques such as thermal evaporation [14, 15] and a two-step sequential solution processing [16-18]. The efficiency of ICLB-based perovskite solar cells reached as high as 10.45 % using the thermal evaporation method [14]. However, this technique required a high vacuum process, which led to a high perovskite solar cell cost. The two-step sequential solution process, which is a low cost one, was applied for preparing the ICLB films. The ICLB-based solar cell performance fabricated with this technique by Sutton *et al*. [18] reach 9.8% in the best cell, and cells performance with 5.6% stabilized power output was demonstrated. Chang *et al*. [16] reported that the efficiency of the ICLB-based solar cells decreased by only 11.7% of the initial value after 250 h. Liang *et al*. [19] found that the performance of ICLB-based PSCs without an encapsulation showed almost no decrease in humid air (90-95% RH, 25°C) after 3 months (2640 h), and the cells could endure extreme high (100°C) and low (-22°C) temperatures.

Among the ICLB perovskite-based compounds ($CsPbBr_3$ [13-15], $CsPbI_2Br$ [18], $CsPb_2Br_5$ [20], Cs_4PbBr_6 [21]), $CsPbBr_3$ appears to be the most suitable candidate for solar cell application because it has the lowest E_g value (1.81 eV) [22, 23] compared with E_g ~ 3.08 eV for $CsPb_2Br_5$ [20] and E_g ~ 3.90 eV for Cs_4PbBr_6 [21]. However, the experimental E_g reported in the literatures is about 2.4 eV. This could have been because the perovskite film may have contained nanometer-sized crystals, which have an experimental E_g value larger than the theoretical value [21, 24]. $CsPbBr_3$ perovskite film has a direct bandgap and a high absorption coefficient. Unfortunately, it is difficult to prepare pure $CsPbBr_3$ phase because the ratio of CsBr and $PbBr_2$ must be properly controlled. An excess of CsBr results in the co-existence of Cs_4PbBr_6 phase, but an excess of $PbBr_2$ induces $CsPb_2Br_5$ formation. Cs_4PbBr_6 and $CsPb_2Br_5$ are unsuitable for solar cell applications because of their high E_g values. Thus, controlling the process during $CsPbBr_3$ film preparation is a very important factor in obtaining pure $CsPbBr_3$ film and high solar cell efficiency. Zhang *et al*. [25] reported that small presence of $CsPb_2Br_5$ phase in the $CsPbBr_3$ perovskite films had a positive effect on efficiency and stability. $CsPb_2Br_5$ could reduce surface defects, charge carrier recombination, and it is more stable against humidity and temperature than pure $CsPbBr_3$ film.

In this work, we focused on the influence of the CsBr concentrations on ICLB film formation, surface morphology and phase composition. The ICLB perovskite films were prepared via the two-step sequential solution method. The ICLB-based perovskite solar cells were assembled using carbon film as the back electrode without hole transport materials (HTM-free). The effects of CsBr concentration on solar cell performance and stability were investigated in detail.

2. Materials and Methods

The perovskite solar cell was composed of the electron transport layer (ETL), perovskite layer, hole transport material layer (HTM), and back contact electrode. The details of preparation of each layer are described below.

2.1 Preparation of the electron transport layer

TiO_2 film was used as the electron transport material layer. In this type of perovskite solar cell, two types of TiO_2 were used. First, the TiO_2 blocking layer (TiO_2-BL, dense TiO_2 film) was coated on the F- doped SnO_2 (FTO) conductive substrate, which functions as the ETL layer and is used for prevent a short circuit between the back electrode and FTO substrate. The second type of TiO_2 film was a porous TiO_2 layer (TiO_2-porous), coated on the TiO_2-BL layer. The role of this layer is also an ETL layer which conducts the exited state electrons from the perovskite material to the conducting substrate. Moreover, the TiO_2-porous layer can cause an increase of the contact area between perovskite layer and ETL layer. The details of the ETL film preparation are described below.

FTO transparent conducting substrates with a size of 2.0 cm x 2.0 cm were cleaned using detergent solution, deionized (DI) water, and ethyl alcohol in an ultra-sonic bath for 20 min, and then dried in hot air. After that, each cleaned FTO substrate was treated in a UV-Ozone system for 10 min to remove any residual organic compound. The TiO_2 blocking layer (TiO_2-BL) was prepared by the spin coating technique. A mixture of 40 ml titanium diisopropoxide bis (acetylacetonate), 1 ml de-ionized water, 40 ml ethanol, 0.5 ml highly concentrated HCL, and 0.5 ml highly concentrated HNO_3 solutions was used as the starting precursor and coated on each cleaned FTO substrate. The spinning speeds and times were set at 2000 rpm for 30 s and 4000 rpm for 60 s, respectively. After coating, it was heated at 80°C for 10 min. Finally, the coated films were annealed at 550°C for 2 h then cooled down to room temperature. The TiO_2-porous layer was prepared by the spin coating technique. This porous layer was coated on the TiO_2-BL layer using a mixture of 1.654 g TiO_2 commercial paste (PST-18NR, Dye-sol) diluted with 6 ml ethanol. The coating speed and times were set at 4000 rpm for 60 s. After spinning, the films were dried at 80°C for 10 min on a hot plate. After that, the dried films were annealed at 550°C for 2 h and then allowed to cool down to room temperature.

2.2 Preparation of the Inorganic Cesium Lead Bromide perovskite films

The ICLB perovskite films were prepared by a two-step sequential solution process under open-air conditions. Firstly, 1.4 M $PbBr_2$ was dissolved in a mixture of dimethylformamide (DMF) and dimethyl sulfoxide (DMSO) with a ratio of 9:1 v/v. The $PbBr_2$ film was coated on the TiO_2-porous layer by the spin coating method. The spinning speed and times were set as 4000 rpm and 60 s. The coated $PbBr_2$ film was dried at 80°C for 10 min on a hot plate. Then, it was immersed in a CsBr solution (CsBr dissolved in methanol) at various concentrations of 0.04, 0.06, 0.08, 0.10, and 0.12 M. During the immersion, the temperature was kept at 50°C and the dipping time was set at 20 min. Finally, the immersed films were heated at 150°C in ambient air for 10 min. After cooling down to room temperature, the ICLB perovskite film was formed with a yellow-orange color. The ICLB perovskite film preparation method is shown in Figure 1.

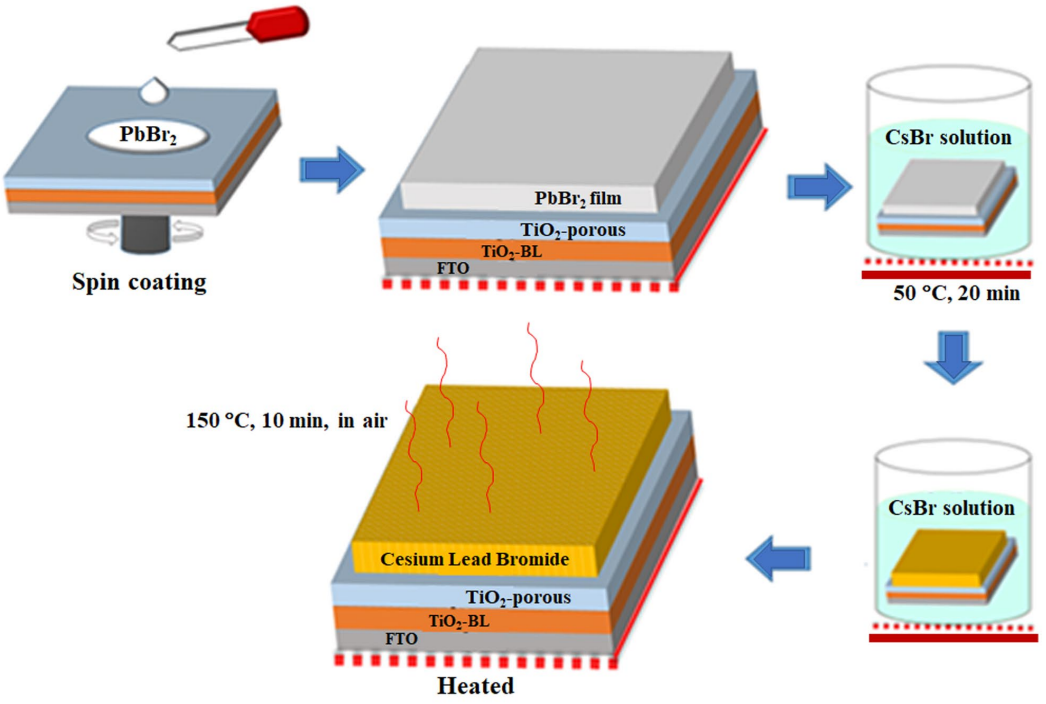

Figure 1. Schematic diagram of the ICLB perovskite film preparation using a two-step sequential solution method

2.3 The back electrode preparation and perovskite solar cells assembly

Carbon films were used as the back electrode and HTM free layers. Firstly, carbon paste was prepared by mixing 6.0 g graphite platelet, 3.0 g of carbon black, and 2.5 g of polyvinyl acetate (PVAc) in 30 ml of ethyl acetate. After mixing well, the ethyl acetate solution was evaporated completely by heating at 80°C for several hours. Then chlorobenzene (CB) was filled into the dried media and stirred until a well-mixed carbon paste resulted. The carbon films were coated onto the FTO/TiO_2-BL/TiO_2-porous/perovskite samples using a doctor blade technique. After coating, the carbon films were heated at 80°C for 10 min then cooled to room temperature. The final perovskite solar cell structure was FTO/TiO_2-BL/TiO_2-porous/perovskite/carbon as shown in Figure 2. The solar cell exposure area used in this experiment was set at 1.0 cm^2.

2.4 Characterizations

The surface morphology and the thickness of ICLB perovskite films were characterized using scanning electron microscope (SEM). The crystalline structure and light absorption properties of these films were investigated using X-ray Diffractometer (XRD) and ultra-violet visible absorption spectroscopy (UV-vis), respectively. The solar cell performance was tested by the solar simulator (PEC-L11) under A.M. 1.5 light spectrum at room temperature. The J-V characteristic curves were measured by a Keithley-2400 series SMU instrument. The solar cell efficiency (η) was calculated from the J-V curve using equation (1).

$$\eta = \frac{J_{sc} \times V_{oc} \times FF}{P_{in}} \times 100\% \quad (1)$$

Where J_{sc} is the short circuit current density, V_{oc} is the open circuit voltage, FF is the fill factor, and P_{in} is the input photon intensity from the standard light source.

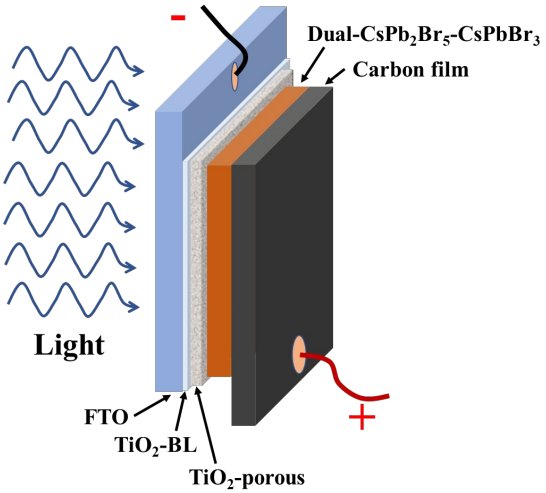

Figure 2. The ICLB perovskite solar cell structure

3. Results and Discussion

The crystalline structure of the ICLB films prepared by the two-step sequential solution with various CsBr concentrations (0.04, 0.06, 0.08, 0.10 and 0.12 M) was characterized by XRD and the results are shown in Figure 3. The XRD spectra of the perovskite films prepared from 0.04, 0.06, 0.08, and 0.10 M CsBr concentrations revealed that the films were composed of mixed phases of tetragonal $CsPb_2Br_5$ (JCPDS No. 00-025-0211) and monoclinic $CsPbBr_3$ (JCPDS No. 00-018-0364). However, the 0.12 M CsBr concentration sample was composed of three mixed phases: tetragonal $CsPb_2Br_5$, monoclinic $CsPbBr_3$, and rhombohedral Cs_4PbBr_6 (JCPDS No. 01-073-2478). The tetragonal $CsPb_2Br_5$ phase can form under rich $PbBr_2$ conditions as illustrated in equation (2) [26]. While the tetragonal $CsPb_2Br_5$ interacts with CsBr converting into the monoclinic $CsPbBr_3$, as shown in equation (3). A small peak of the rhombohedral Cs_4PbBr_6 appears under the 0.12 M CsBr condition. This is likely due to $CsPbBr_3$ reacting with the excessive CsBr, as illustrated in equation (4) [26]. It is worth noting that the 0.08 M CsBr concentration resulted in the lowest remaining $PbBr_2$ (at 18.5°) and the rhombohedral Cs_4PbBr_6 phase did not appear. There was a co-existence of $CsPb_2Br_5$ (002) at 2θ ~11.7° and $CsPbBr_3$ (200) at 2θ ~30.7° on ICLB_0.08M films. The main phases of the ICLB_0.08M sample were the tetragonal $CsPb_2Br_5$ and the monoclinic $CsPbBr_3$. The co-existence of the $CsPb_2Br_5$ and $CsPbBr_3$ on the ICLB_0.08M sample should be of benefit to the solar cell performance because $CsPb_2Br_5$ can reduce surface defects and charge carrier recombination, and it is stable against humidity and temperature [25]. The high CsBr concentration can cause $PbBr_2$ to remain and rhombohedral Cs_4PbBr_6 formation. These effects in turn have negative effects on solar

cell efficiency because of the high energy bandgap of $PbBr_2$ and Cs_4PbBr_6 (E_g ~ 4.2 eV for $PbBr_2$ [27], and E_g ~ 3.90 eV for Cs_4PbBr_6 [21, 24]).

$$2PbBr_2 + CsBr \rightarrow CsPb_2Br_5 \text{ (with excess amount of } PbBr_2) \quad (2)$$

$$CsPb_2Br_5 + CsBr \rightarrow 2CsPbBr_3 \text{ (with excess amount of CsBr)} \quad (3)$$

$$CsPbBr_3 + 3CsBr \rightarrow Cs_4PbBr_6 \text{ (with excess amount of CsBr)} \quad (4)$$

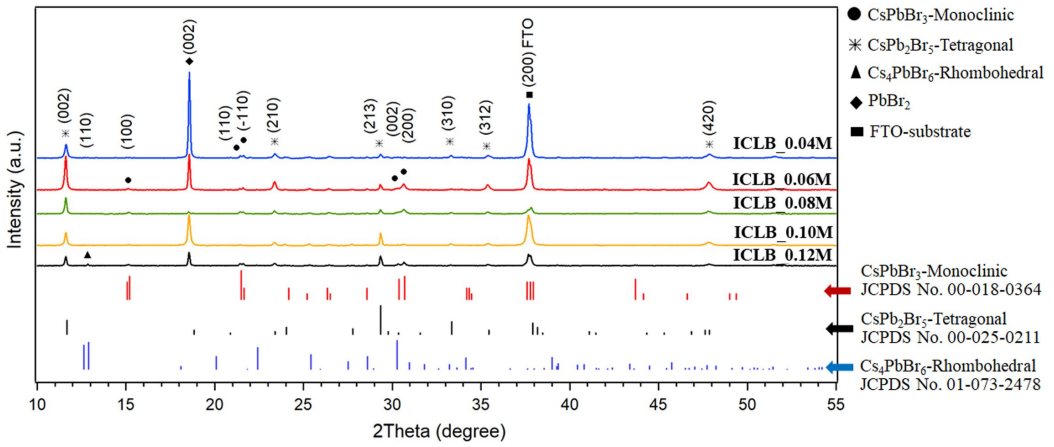

Figure 3. X-ray diffraction spectra of the ICLB perovskite films prepared from the different CsBr concentrations, and the standard $CsPbBr_3$, $CsPb_2Br_5$ and Cs_4PbBr_6 structures

Figure 4 shows the surface morphology and cross-section images of ICLB perovskite films. It can be seen that the ICLB_0.04, ICLB_0.06 and ICLB_0.08M samples have a particle size of approximately 1.0 µm with the tetragonal shape, but the ICLB_0.10 and ICLB_0.12 M samples have large and irregular shaped particles. In addition, the ICLB-0.08M sample has a denser crystalline surface than those of the other samples, as seen in Figure 4c. This is probably the result of the CsBr concentration being suitable for perovskite crystallization. Crystal heterogeneity on the ICLB_0.12M sample in Figure 4e may be due to the formation of rhombohedral Cs_4PbBr_6 phase. The thicknesses of the ICLB perovskite films estimated from the cross-sectional images (the film thickness was measured from 20 different point on the cross-sectional images) are listed in Table 1. The film thickness increases with increasing CsBr concentration from 0.04 M to 0.08 M. This is likely due to the increasing interaction of CsBr with $PbBr_2$ film. However, the thicknesses of the ICLB_0.10M and ICLB_0.12M films are lower than that of the ICLB_0.08M sample. This may be attributed to the incomplete reaction between $PbBr_2$ and CsBr, which is evidenced by the appearance of the (002) plane of $PbBr_2$ in the XRD spectrum shown in Figure 3.

UV-vis absorption spectra of ICLB films are illustrated in Figure 5a. All absorption spectra show a clear first absorption edge at the wavelength at 530 nm and a second absorption edge around 350-400 nm. The absorbance peak at 530 nm corresponds to the $CsPbBr_3$ phase, while the absorption peak around 350-400 nm corresponds to the $CsPb_2Br_5$ structure. The ICLB_0.08M sample has the highest absorbance because it is the thickest film and the low $PbBr_2$ remaining. The direct optical energy bandgap (E_g) of the $CsPbBr_3$ perovskite films are estimated from Tauc relation using equation (5) [28, 29].

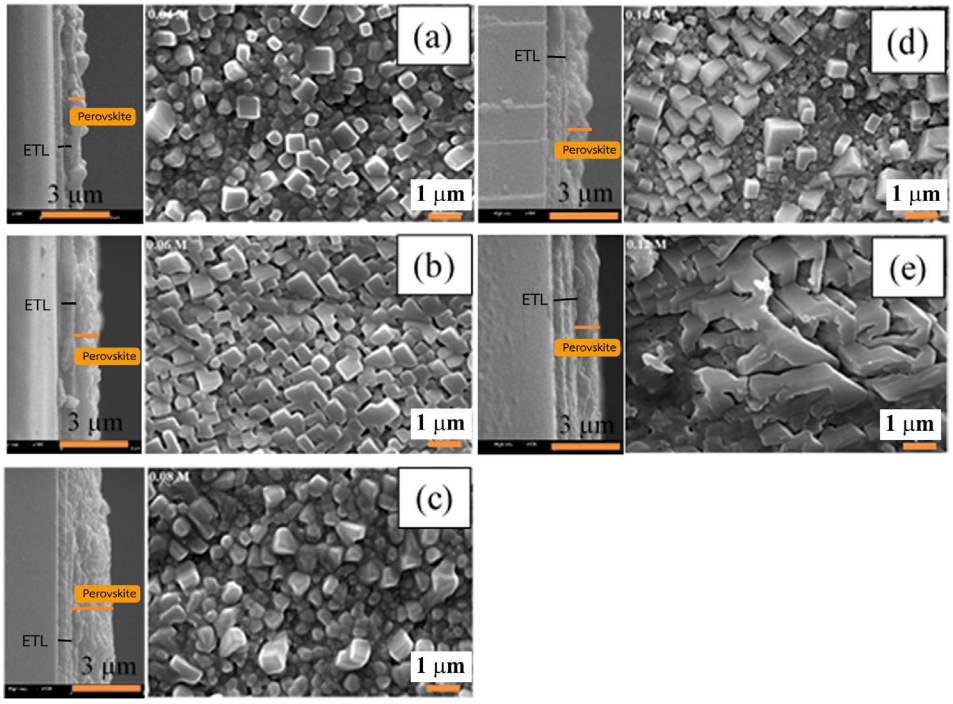

Figure 4. Cross-section and surface morphology SEM images of the ICLB perovskite films coated on the FTO substrate prepared from the different CsBr concentrations, (a) ICBL_0.04 M, (b) ICBL_0.06 M, (c) ICBL_0.08 M, (d) ICBL_0.10 M, and (e) ICBL_0.12 M

$$(\alpha hv)^2 = \beta^2(hv - E_g) \quad (5)$$

Where, β is a constant. α, h and v are the absorption coefficient, Planck's constant, and the photon frequency, respectively. The direct optical bandgaps of the ICLB films were determined by extrapolating the linear regions to the photon energy axis as illustrated in Figure 5b. E_g values of all samples are around 2.28-2.35 eV as listed in Table 1, which contributed to the presence of nanocrystal $CsPbBr_3$ in the film [24, 30]. However, the indirect optical bandgap of $CsPb_2Br_5$ evaluated from the plot of $(\alpha hv)^{1/2}$ versus photon energy (hv) in Figure 5c done according to equation (6) was approximately 2.87-3.10 eV (as summarized in Table 1). This value is close to the tetragonal $CsPb_2Br_5$ phase (~3.08 eV) [31]. The ICLB_0.04M sample had the highest E_g value (3.5 eV) among five samples. This may be due to the large amount of $PbBr_2$ remaining on film as evidenced by XRD spectrum in Figure 3.

$$(\alpha hv)^{1/2} = \beta^{1/2}(hv - E_g) \quad (6)$$

The HTM-free perovskite solar cells were assembled using the ICLB films as the light absorber, and the carbon film as the hole-collector. The structure of this carbon-based HTM-free ICLB perovskite solar cells was as follows: FTO/TiO_2-BL/TiO_2-porous/dual-$CsPb_2Br_5$-$CsPbBr_3$/carbon film as illustrated in schematic Figure 2. The photocurrent density (J) versus photovoltage (V) curves are shown in Figure 6. The short circuit current density (J_{sc}), open circuit

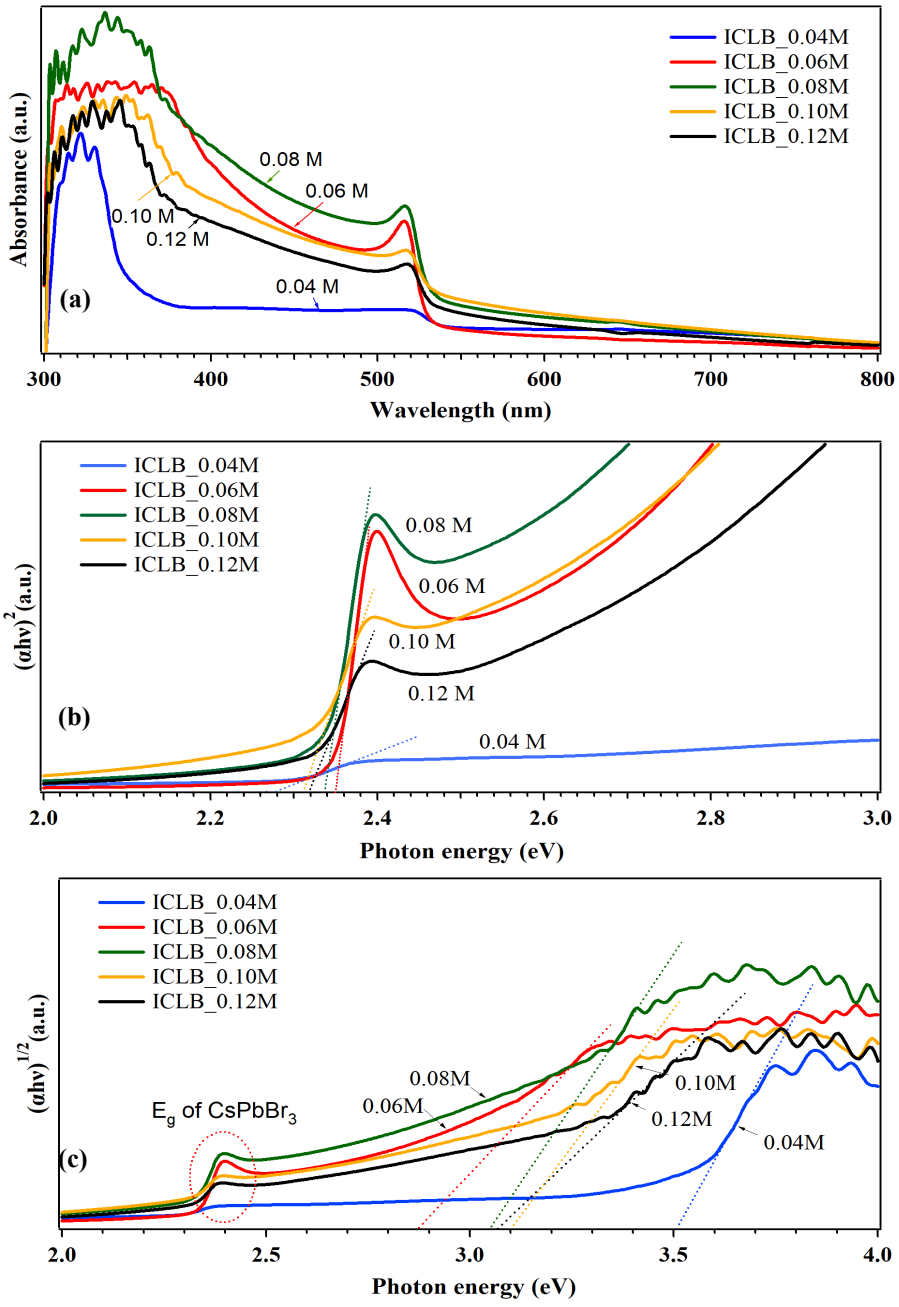

Figure 5. UV-vis absorption spectra of the ICLB perovskite films, (a) absorbance, (b) the estimation of the direct optical energy bandgap of $CsPbBr_3$, and (c) the estimation of the indirect optical energy bandgap of $CsPb_2Br_5$

Table 1. Films thickness and energy bandgap of the ICLB films, and the photovoltaic parameters of the carbon-based HTM-free ICLB perovskite solar cells

Samples	Thickness (µm)	Direct optical bandgap (eV)	Indirect optical bandgap (eV)	J_{sc} (mA cm^{-2})	V_{oc} (V)	FF	η (%)
ICLB_0.04M	0.76 ± 0.12	2.28	3.50	2.92	1.090	0.464	1.50
ICLB_0.06M	0.99 ± 0.11	2.35	2.87	3.23	1.068	0.507	1.70
ICLB_0.08M	1.64 ± 0.18	2.34	3.05	3.83	1.111	0.612	2.60
ICLB_0.10M	0.93 ± 0.13	2.31	3.10	2.39	0.942	0.311	0.70
ICLB_0.12M	1.01 ± 0.08	2.32	3.05	1.61	0.158	0.250	0.10

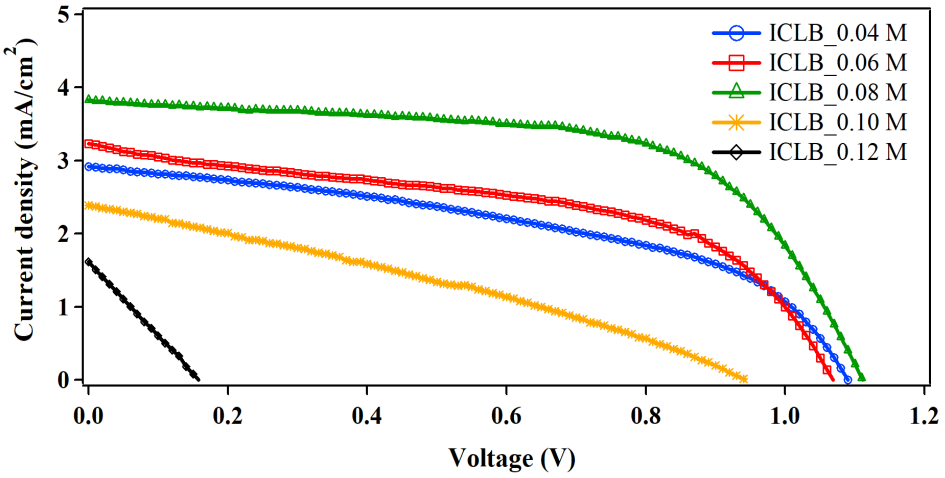

Figure 6. J-V characteristic curves of the carbon-based HTM-free ICLB perovskite solar cells

voltage (V_{oc}), fill factor (FF), and efficiency (η) were extracted from the J-V curves and listed in Table 1. It was found that the values of J_{sc}, V_{oc}, FF and efficiency increased with increasing CsBr concentration in the range of 0.04-0.08 M. This was because the film thickness, absorbance and uniformity of the ICLB perovskite films increased as seen in the UV-visible absorption and SEM results. The high absorbance increases the probability of electron-hole carrier generation. High film uniformity can reduce the carrier recombination rate resulting in the high V_{oc} values [32]. However, the high CsBr concentrations over 0.08 M caused the reduction of J_{SC}, FF, and efficiency. This is owing to the heterogeneity of the perovskite structures and the large remaining $PbBr_2$ impurities in the film. Thus, the optimum condition for preparing the ICLB perovskite film was 0.08 M CsBr concentration, which delivered the highest J_{sc}, V_{oc}, FF, and efficiency of 3.83 mA/cm^2, 1.111 V, 0.612, and 2.60%, respectively.

The stability of the ICLB perovskite solar cells was tested under the ambient environmental conditions, i.e. at room temperature without controlling humidity. Figures 7a-7d reveal that the ICLB perovskite solar cells prepared from the different CsBr concentrations had great cell stability. ICLB cells have the high stability because ICLB film is an inorganic compound, which is well known to have a good resistance to moisture and temperature [33]. The ICLB_0.08M perovskite solar cells exhibited high J_{sc}, V_{oc}, FF, and η stability. The solar cell efficiency was reduced by only 10% of the maximum value (3.0%) after 816 h testing. This good ICLB_0.08M perovskite solar cell stability is probably due to the stable $CsPb_2Br_5$ and $CsPbBr_3$ structures, the uniform crystalline surface and the low $PbBr_2$ impurity phase [34].

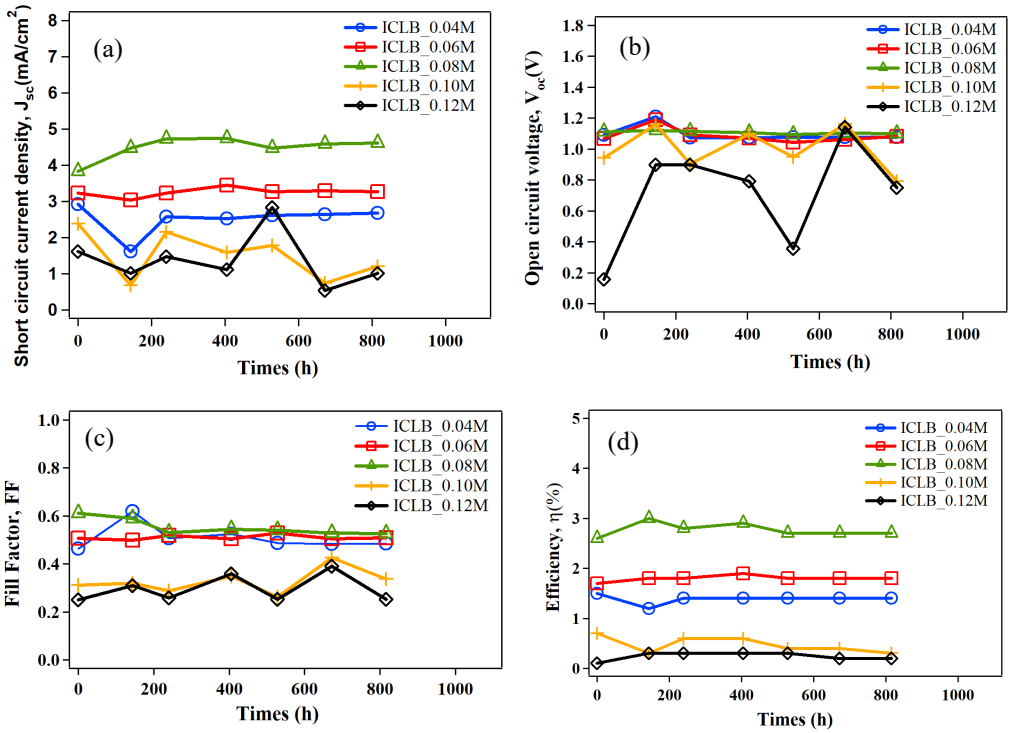

Figure 7. The plots of the (a) J_{sc}, (b) V_{oc}, (c) FF and (d) efficiency of the carbon-based HTM-free ICLB perovskite solar cell versus times

4. Conclusions

ICLB perovskite films were successfully prepared via a two-step sequential solution method in an ambient environment. All ICLB samples were composed of mixed $CsPb_2Br_5$ and $CsPbBr_3$ phases with some $PbBr_2$ impurities. The ICLB_0.08M film showed uniform particle size, low pin-hole defect, low $PbBr_2$ impurities and high light absorbance. The ICLB_0.08M perovskite solar cell delivered the highest efficiency of 2.60% with good cell stability over 816 h. Furthermore, the co-existence of $CsPb_2Br_5$ and $CsPbBr_3$ perovskite showed good potential for converting light energy into electricity. However, its efficiency must be improved for practical applications in the future.

5. Acknowledgements

This work was financially supported by the Department of Physics, Faculty of Science, Buriram Rajabhat University, Thailand, and partially supported by the Department of Physics, Faculty of Science, Khon Kaen University, Thailand, and by the Institute of Nanomaterials Research and Innovation for Energy (IN-RIE), Research Network of NANOTEC-KKU (RNN), Khon Kaen University, Thailand. It was also supported by the Thailand Center of Excellence in Physics (ThEP) and by the National Research Council of Thailand (NRCT-2562, 6200078).

References

[1] Kojima, A., Teshima, K., Shirai, Y. and Miyasaka, T., 2009. Organometal halide perovskites as visible-light sensitizers for photovoltaic cells. *Journal of the American Chemical Society*, 131, 6050-6051.

[2] Im, J.H., Lee, C.R., Lee, J.W., Park, S.W. and Park, N.G., 2011. 6.5% efficient perovskite quantum-dot-sensitized solar cell. *Nanoscale*, 3, 4088-4093.

[3] Kim, H.S., Lee, C.R., Im, J.H., Lee, K.B., Moeh T., Marchioro, A., Moon, S.J., Humphry-Baker, R., Yum, J.H., Moser, J.E., Gratzel, M. and Park, N.G., 2012. Lead iodide perovskite sensitized all-solid-state submicron thin film mesoscopic solar cell with efficiency exceeding 9%. *Scientific Reports*, 2, 591-597.

[4] Burschka, J., Pellet, N., Moon, S.J., Humphry-Baker1, R., Gao1, P., Nazeeruddin, M.K. and Gratzel, M., 2013. Sequential deposition as a route to high-performance perovskite-sensitized solar cells. *Nature*, 499, 316-319.

[5] Zhou, H., Chen, Q., Li, G., Luo, S., Song, T., Duan, H.S., Hong, Z., You, J., Liu, Y. and Yang, Y., 2014. Interface engineering of highly efficient perovskite solar cells. *Science*, 345, 542-546.

[6] Yang, W.S., Noh, J.H., Jeon, N.J., Kim, Y.C., Ryu, S., Seo, J. and Seok, S., 2015. High-performance photovoltaic perovskite layers fabricated through intramolecular exchange. *Science*, 348, 1234-1237.

[7] Bi, D., Tress, W., Dar, M.I., Gao, P., Luo, J., Renevier, C., Schenk, K., Abate, A., Giordano, F., Baena, J.P.C., Decoppet, J.D., Zakeeruddin, S.M., Nazeeruddin, M.K., Gratzel, M. and Hagfeldt, A., 2016. Efficient luminescent solar cells based on tailored mixed-cation perovskites. *Science Advances, 2*, 1501170, https://doi.org/10.1126/sciadv.1501170.

[8] Li, X., Bi, D., Yi, C., Décoppet, J.D., Luo, J., Zakeeruddin, S.M., Hagfeldt, A. and Grätzel M., 2016. A vacuum flash-assisted solution process for high-efficiency large-area perovskite solar cells. *Science*, 353, 58-62.

[9] Green, M.A., Dunlop, E.D., Hohl-Ebinger, J., Yoshita, M., Kopidakis, N. and Ho-Baillie, A.W.Y., 2020. Solar cell efficiency tables (version 55). *Progress in Photovoltaics*, 28, 3-15.

[10] Niu, G., Li, W., Meng, F., Wang, L., Dong, H. and Qiu, Y., 2014. Study on the stability of $CH_3NH_3PbI_3$ films and the effect of post-modification by aluminum oxide in all-solid-state hybrid solar cells. *Journal of Materials Chemistry A*, 2, 705-710.

[11] Wang, Z., Chenab, B. and Rogach, A.L., 2017. Synthesis, optical properties and applications of light-emitting copper nanoclusters. *Nanoscale Horizons*, 62, 135-146.

[12] Zhang, X., Xu, B., Zhang, J., Gao, Y., Zheng, Y., Wang, K. and Sun, W., 2016. All-inorganic perovskite nanocrystals for high-efficiency light emitting diodes: dual-phase $CsPbBr_3$-$CsPb_2Br_5$ composites. *Advanced Functional Materials*, 26, 4595-4600.

[13] Wang, H.C., Lin, S.Y., Tang, A.C., Singh, B.P., Tong, H.C., Chen, C.Y., Lee, Y.C., Tsai, T.L. and Liu, R.S., 2016. Mesoporous silica particle integrated with all-inorganic $CsPbBr_3$

perovskite quantum-dot nanocomposite (MP-PQDs) with high stability and wide color gamut used for backlight display. *Angewandte Chemie International Edition*, 55, 8056-8061.

[14] Li, J., Gao, R., Gao, F., Lei, J., Wang, H., Wu, X., Li, J., Liu, H., Hua, X. and Liu, S.F., 2019. Fabrication of efficient $CsPbBr_3$ perovskite solar cells by single-source thermal evaporation. *Journal of Alloys and Compounds*, 818, 152903, https://doi.org/10.1016/j.jallcom.2019.152903.

[15] Li, X., Tan, Y., Lai, H., Li, S., Chen, Y., Li, S., Xu, P. and Yang. J., 2019. All-inorganic CsPbBr3 perovskite solar cells with 10.45% efficiency by evaporation-assisted deposition and setting intermediate energy levels. *ACS Applied Materials and Interfaces*, 11, 29746-29752.

[16] Chang, X., Li, W., Zhu, L., Liu, H., Geng, H., Xiang, S., Liu J. and Chen, H., 2016. Carbon-based $CsPbBr_3$ perovskite solar cells: all-ambient processes and high thermal stability. *ACS Applied Materials and Interfaces*, 8, 33649-33655.

[17] Kulbak, M., Gupta, S., Kedem, N., Levine, I., Bendikov, T., Hodes, G. and Cahen, D., 2016. Cesium enhances long-term stability of lead bromide perovskite-based solar cells. *The Journal of Physical Chemistry Letters*, 7, 167-172.

[18] Sutton, R.J., Eperon, G.E., Miranda, L., Parrott, E.S., Kamino, B.A., Patel, J.B., Horantner, M.T., Johnston, M.B., Haghighirad, A.A., Moore, D.T. and Snaith, H.J., 2016. Bandgap-tunable cesium lead halide perovskites with high thermal stability for efficient solar cells. *Advanced Energy Materials*, 6, 1502458, htpps://doi.org/10.1002/aenm.201502458.

[19] Liang, J., Wang, C., Wang, Y., Xu, Z., Lu, Z., Ma, Y., Zhu, H., Hu, Y., Xiao, C., Yi, X., Zhu, G., Lv, H., Ma, L., Chen, T., Tie, Z., Jin, Z. and Liu, J., 2016. All-inorganic perovskite solar cells. *Journal of the American Chemical Society*, 138, 15829-15832.

[20] Li, J., Zhang, H., Wang, S., Long, D., Li, M., Guo, Y., Zhong, Z., Wu, K., Wang, D. and Zhang, T., 2017. Synthesis of all-inorganic $CsPb_2Br_5$ perovskite and determination of its luminescence mechanism. *RSC Advances*, 7, 54002-54007.

[21] Wang, L., Liu, H., Zhang, Y. and Mohammed, O.F., 2020. Photoluminescence origin of zero dimensional Cs_4PbBr_6 perovskite. *ACS Energy Letters*, 5, 87-99.

[22] Murtaza, G. And Ahmad, I., 2011. First principle study of the structural and optoelectronic properties of cubic perovskites $CsPbM_3$ (M= Cl, Br, I). *Physica B Condensed Matter*, 406, 3222-3229.

[23] Qian, J., Xu, B. and Tian, W.A., 2016. Comprehensive theoretical study of halide perovskites ABX_3. *Organic Electronics*, 37, 61-73.

[24] Yang, L., Wang, T., Min, Q., Liu, B., Liu, Z., Fan, X., Qiu, J., Xu, X., Yu, J. and Yu, X., 2019. High water resistance of monoclinic $CsPbBr_3$ nanocrystals derived from zero-dimensional cesium lead halide perovskites. *ACS Omega*, 4, 6084-6091.

[25] Zhang, X., Jin, Z., Zhang, J., Bai, D., Bian, H., Wang, K., Sun, J., Wang, Q. and Liu, S.F., 2018. All-ambient processed binary $CsPbBr_3$–$CsPb_2Br_5$ perovskites with synergistic enhancement for high-efficiency Cs–Pb–Br-based solar cells. *ACS Applied Materials and Interfaces*, 10, 7145-7154.

[26] Duan, J., Zhao, Y., He, B. and Tang, Q., 2018. High-purity inorganic perovskite films for solar cells with 9.72% efficiency. *Angewandte Chemie International Edition*, 57, 3787-3791.

[27] Eijkelenkamp, A.J.H. and Vos, K., 1976. Reflectance measurements on single crystals of PbFCl, PbFBr, and $PbBr_2$. *Physica Status Solidi (b),* 76, 769-778.

[28] Tauc, J., 1968. Optical properties and electronic structure of amorphous Ge and Si. *Materials Research Bulletin*, 3, 37-46.

[29] Kortüm, G., Braun, W. and Herzog, G., 1963. Principles and techniques of diffuse-reflectance spectroscopy. *Angewandte Chemie International Edition,* 2, 333-341.

[30] Maes, J., Balcaen, L., Drijvers, E., Zhao, Q., De Roo, J., Vantomme, A., Vanhaecke, F., Geiregat, P. and Hens, Z., 2018. Light absorption coefficient of $CsPbBr_3$ perovskite nanocrystals. *The Journal of Physical Chemistry Letters*, 9, 3093-3097.

[31] Dursun, I., Bastiani, M.D., Turedi, B., Alamer, B., Shkurenko, A., Yin, J., El-Zohry, A.M., Gereige, I., AlSaggaf, A., Mohammed, O.F., Eddaoudi, M. and Bakr, O.M., 2017. $CsPb_2Br_5$ single crystals :Synthesis and characterization. *ChemSusChem Communications*, 10, 3746-3749.

[32] Tang, M., He, B., Dou, D., Liu, Y., Duan, J., Zhao, Y., Chen, H. and Tang, Q., 2019. Toward efficient and air-stable carbon-based all-inorganic perovskite solar cells through substituting $CsPbBr_3$ films with transition metal ions. *Chemical Engineering Journal*, 375, 121930, https://doi.org/10.1016/j.cej.2019.121930.

[33] Kumar, N., Rani, J. and Kurchania, R. 2021. Advancement in $CsPbBr_3$ inorganic perovskite solar cells: Fabrication, efficiency and stability. *Solar Energy*, 221, 197-205.

[34] Li, Y., Yang, X. and Xie, A., 2021. Preparation of surface modified $CsPbBr_3$@$CsPb_2Br_5$ nanocrystals with high stability by a pseudo-peritectic method. *Journal of Luminescence*, 236, 118154, https://doi.org/10.1016/j.jlumin.2021.118154.